Dispersion imaging spectrometer for detecting and locating energetic targets in real time

Qinghua Yang (杨庆华)[1*], Xiaodong Zeng (曾晓东)[1], and Baochang Zhao (赵葆常)[2]

[1]*School of Technical Physics, Xidian University, Xi'an 710071, China*

[2]*Xi'an Institute of Optics and Precision Mechanics, Chinese Academy of Sciences, Xi'an 710119, China*

[*]*Corresponding author: yangqh666@163.com*

Received January 19, 2013; accepted February 25, 2013; posted online May 30, 2013

A conceptual dispersion imaging spectrometer (DIS) is proposed. It consists of a telescope, four prisms, an imaging lens, and a detector. The first prism allows only the first set of wavelengths along the first direction to pass and disperse. The second prism allows only the second set of wavelengths along the second direction, which is perpendicular to the first. The third and fourth prisms are used to compensate for the angular deviations from the optical axes of the first and second prisms, respectively. The proposed DIS disperses the spectra of a target to form an L-shaped dispersion pattern (LDP). The theoretical calculation and numerical simulation of the LDP are presented. The DIS can locate multiple targets based only on data obtained from a single frame. It is suitable for detecting and locating energetic targets in real time.

OCIS codes: 120.6200, 230.5480, 300.6190, 120.4640.

doi: 10.3788/COL201311.061202.

Real-time or near real-time detection and measurement of energetic targets are becoming more important in military and commercial applications, such as tactical or strategic missile threat warning, battlefield characterization (e.g., location of artillery threats), and small arms or sniper fire detection and location. In all these cases, threats or targets may be unscheduled or unannounced. Other unknown energetic targets may also rapidly evolve in time. Thus, simultaneous and rapid sampling of spectral bands within the target spectra is important. Conventional imaging spectrometers, such as scanned slit, filter, and Fourier transform spectrometers[1−18], use scanning techniques to multiplex the three-dimensional (3D) spectral image (i.e., two spatial dimensions and one spectral dimension) onto a two-dimensional (2D) detector. These spectrometers can characterize the spectral signature of the target that is static in time. Given that energetic targets rapidly evolve in time, conventional techniques do not have enough time to scan. Furthermore, the location of the energetic target may be unknown. Therefore, conventional imaging spectrometers cannot detect and locate unannounced energetic targets in real time.

The angularly multiplexed spectral imager proposed by Mooney *et al.*, based on a rotating direct-vision prism, requires at least two frames of data to locate the target[19−24]. Thus, it cannot locate energetic targets in real time. Moreover, the significance of the data obtained in two temporally separated frames is substantially diminished when a target rapidly moves across the field of view and changes, such that its spectral signature differs between the first and second frames. Therefore, this sensor cannot detect and locate unannounced energetic targets in real time.

This letter reports a dispersion imaging spectrometer (DIS) for detecting and locating energetic targets in real time. Figure 1 shows the optical layout of the DIS, which consists of a telescope, four prisms (prisms 1, 2, 3, and 4), an imaging lens, and a detector. The detector is located in the focal plane of the imaging lens. The first prism (prism 1) disperses only the first set of wavelengths (WL1) along the vertical direction. The second prism (prism 2) disperses only the second set of wavelengths (WL2) along the horizontal direction. Prism 3 compensates for the angular deviation from the optical axis in prism 1. Prism 4 compensates for the angular deviation from the optical axis in prism 2.

The light emitted from a target and transmitted through the telescope becomes the parallel beam. One part of the parallel beam is dispersed by prism 1 along the vertical direction, whereas the other part of the parallel beam is dispersed by prism 2 along the horizontal direction. These dispersed wavelengths are mapped by the imaging lens onto the detector to form an L-shaped dispersion pattern (LDP). Each LDP is a snapshot of the target spectra.

The y-axis coordinate y_i of the imaging position $P_i(x_i, y_i)$ of the dispersed wavelength λ_i within the first wavelength set WL1 can be derived in the meridian plane (Fig. 2). Points A, B, C, and D are the intersections of the ray and surfaces 1, 2, 3, and 4, respectively. E is the intersection of the ray and the lens. D' is the image point of point D with respect to the lens. h_1, h_2, and h'_1 are the y-axis coordinates of points D, E, and D', respectively. d_1 is the distance between point D and the lens, d'_1 is the distance between point D' and the lens, and f is the focal length of the lens. θ_1, θ_2, θ_3, and θ_4 are the angles of refraction in the meridian plane of the ray on surfaces 1, 2, 3, and 4, respectively. ϕ is the angle of incidence in the meridian plane of the ray to prism 1. α is the vertex angle of prism 1. γ_1 is the vertex angle of prism 3. $n_1(\lambda_i)$ is the refractive index of prism 1 for wavelength λ_i. $n_3(\lambda_i)$ is the refractive index of prism 3 for wavelength λ_i.

According to the geometrical relationship in Fig. 2 and the imaging formula of the lens, we can obtain

$$\frac{h_2 - y_i}{h_2 - h'_1} = \frac{f}{d'_1}, \tag{1a}$$

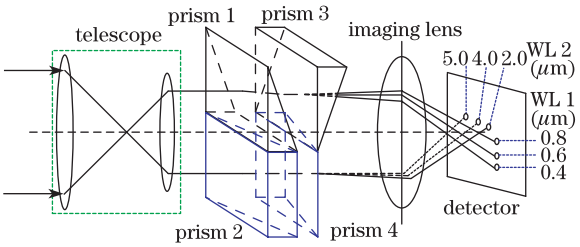

Fig. 1. Optical layout of the DIS.

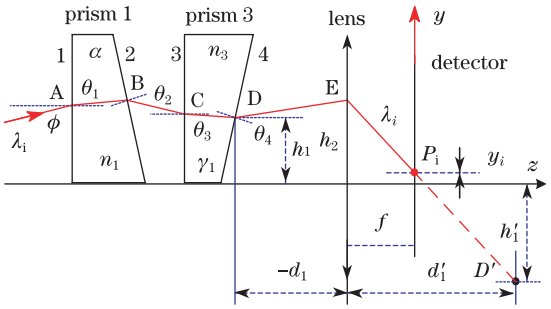

Fig. 2. Ray tracing in the meridian plane.

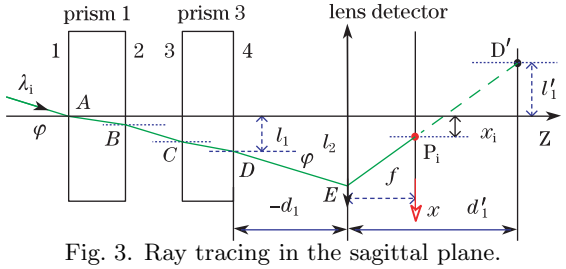

Fig. 3. Ray tracing in the sagittal plane.

$$\frac{1}{d_1'}-\frac{1}{-d_1}=\frac{1}{f}, \tag{1b}$$

$$\frac{h'_1}{h_1}=\frac{d_1'}{-d_1}, \tag{1c}$$

$$h_2=h_1+d_1\tan\left(\theta_4-\gamma_1\right). \tag{1d}$$

According to the law of refraction, we can obtain

$$\sin\phi=n_1\left(\lambda_i\right)\sin\theta_1, \tag{2a}$$

$$n_1\left(\lambda_i\right)\sin\left(\alpha-\theta_1\right)=\sin\theta_2, \tag{2b}$$

$$\sin\left(\theta_2-\alpha\right)=n_3\left(\lambda_i\right)\sin\theta_3, \tag{2c}$$

$$n_3\left(\lambda_i\right)\sin\left(\gamma_1-\theta_3\right)=\sin\theta_4. \tag{2d}$$

Based on Eqs. (1) and (2), the y-axis coordinate y_i can be expressed as

$$y_i=f\frac{n_3\left(\lambda_i\right)\left(\sin\gamma_1\sqrt{1-\psi^2}-\psi\cos\gamma_1\right)-\tan\gamma_1\sqrt{1+n_3^2\left(\lambda_i\right)\left(\psi\sin2\gamma_1\sqrt{1-\psi^2}-\sin^2\gamma_1-\psi^2\cos2\gamma_1\right)}}{\sqrt{1+n_3^2\left(\lambda_i\right)\left(\psi\sin2\gamma_1\sqrt{1-\psi^2}-\sin^2\gamma_1-\psi^2\cos2\gamma_1\right)}+n_3\left(\lambda_i\right)\left(\sin\gamma_1\sqrt{1-\psi^2}-\psi\cos\gamma_1\right)\tan\gamma_1}, \tag{3a}$$

where ψ is

$$\psi=\frac{\sin\alpha\cos\alpha\sqrt{n_1^2\left(\lambda_i\right)-\sin^2\phi}-\cos^2\alpha\sin\phi}{n_3\left(\lambda_i\right)}-\frac{\sin\alpha\sqrt{1+\sin2\alpha\sin\phi\sqrt{n_1^2\left(\lambda_i\right)-\sin^2\phi}-n_1^2\left(\lambda_i\right)\sin^2\alpha-\cos2\alpha\sin^2\phi}}{n_3\left(\lambda_i\right)}. \tag{3b}$$

The x-axis coordinate x_i of the imaging position of the dispersed wavelength λ_i within the first wavelength set WL1 can be derived in the sagittal plane (Fig. 3). l_1, l_2, and l_1' are the x-axis coordinates of points D, E, and D', respectively. φ is the angle of incidence in the sagittal plane of the ray to prism 1.

According to the geometrical relationship in Fig. 3 and the imaging formula of the lens, we can obtain

$$\frac{x_i-l_2}{l_1'-l_2}=\frac{f}{d_1'}, \tag{4a}$$

$$\frac{1}{d_1'}-\frac{1}{-d_1}=\frac{1}{f}, \tag{4b}$$

$$\frac{l_1'}{l_1}=\frac{d_1'}{-d_1}, \tag{4c}$$

$$l_2=l_1+d_1\tan\varphi. \tag{4d}$$

Therefore, the x-axis coordinate x_i can be expressed as

$$x_i=f\tan\varphi. \tag{5}$$

Similarly, the y-axis coordinate y_j of the imaging position of the dispersed wavelength λ_j within the second wavelength set WL2 can be expressed as

$$y_j=f\tan\phi. \tag{6}$$

The x-axis coordinate x_j of the imaging position of the dispersed wavelength λ_j within the second wavelength set WL2 can be expressed as

$$x_j=f\frac{\sqrt{1+n_3^2\left(\lambda_j\right)\left(\kappa\sqrt{1-\kappa^2}\sin2\gamma_2-\sin^2\gamma_2-\kappa^2\cos2\gamma_2\right)}\tan\gamma_2-n_3\left(\lambda_j\right)\left(\sqrt{1-\kappa^2}\sin\gamma_2-\kappa\cos\gamma_2\right)}{\sqrt{1+n_3^2\left(\lambda_j\right)\left(\kappa\sqrt{1-\kappa^2}\sin2\gamma_2-\sin^2\gamma_2-\kappa^2\cos2\gamma_2\right)}+n_3\left(\lambda_j\right)\left(\sqrt{1-\kappa^2}\sin\gamma_2-\kappa\cos\gamma_2\right)\tan\gamma_2}, \tag{7a}$$

where κ is

$$\kappa = \frac{\left(\sqrt{n_2^2(\lambda_j) - \sin^2\varphi}\sin\beta\cos\beta + \sin\varphi\cos^2\beta\right)}{n_3(\lambda_j)} - \frac{\sqrt{1 - n_2^2(\lambda_j)\sin^2\beta - \cos 2\beta\sin^2\varphi - \sin 2\beta\sin\varphi\sqrt{n_2^2(\lambda_j) - \sin^2\varphi}}\sin\beta}{n_3(\lambda_j)}, \tag{7b}$$

where $n_2(\lambda_j)$ is the refractive index of prism 2 for wavelength λ_j, $n_3(\lambda_j)$ is the refractive index of prism 4 for wavelength λ_j, β is the vertex angle of prism 2, and γ_2 is the vertex angle of prism 4.

When the DIS has no prism, the imaging location of a target is called the non-dispersed imaging location (NDIL).

Figure 4 shows a sketch map of imaging in the sagittal plane of a distant target of the DIS without the four prisms. f_1 is the focal length of the telescope objective, f_2 is the focal length of the telescope eyepiece, Φ_1 is the angle of the ray emitted from a target and the optical axis in the sagittal plane, φ is the angle of the emergent ray from the telescope eyepiece and the optical axis in the sagittal plane, and x_0 is the x-axis coordinate of the NDIL. We can obtain

$$x_0 = f\tan\varphi, \tag{8}$$

$$f_1\tan\Phi_1 = f_2\tan\varphi. \tag{9}$$

Similarly, the y-axis coordinate y_0 of the NDIL can be expressed as

$$y_0 = f\tan\phi, \tag{10}$$

$$f_1\tan\Phi_2 = f_2\tan\phi, \tag{11}$$

where ϕ is the angle of the emergent ray from the telescope eyepiece and the optical axis in the meridian plane, and Φ_2 is the angle of the ray emitted from a target and the optical axis in the meridian plane.

If the wavelength sets WL1 and WL2 are the visible range (from 0.4 to 0.8 μm) and infrared range (from 2.0 to 5.0 μm), respectively (Fig. 1), the material for prism 1 may be zinc sulfide (ZnS), the material for prism 2 may be sapphire (Al_2O_3), and the suitable material for prisms 3 and 4 is calcium fluoride (CaF_2).

The formula of refractive index for ZnS can be written as[25]

$$n^2 - 1 = 3.4175 + \frac{1.7396\lambda^2}{\lambda^2 - 0.2677^2}. \tag{12}$$

The formula of refractive index for Al_2O_3 can be written as[25]

$$n^2 - 1 = \frac{1.4313493\lambda^2}{\lambda^2 - 0.0726631^2} + \frac{0.65054713\lambda^2}{\lambda^2 - 0.1193242^2} + \frac{5.3414021\lambda^2}{\lambda^2 - 18.028251^2}. \tag{13}$$

The formula of refractive index for CaF_2 can be written as[25]

$$n^2 - 1 = \frac{0.5675888\lambda^2}{\lambda^2 - 0.050263605^2} + \frac{0.4710914\lambda^2}{\lambda^2 - 0.1003909^2} + \frac{3.8484723\lambda^2}{\lambda^2 - 34.649040^2}, \tag{14}$$

where the unit of wavelengths is micron (μm).

According to Eqs. (3), (5)–(7), and (12)–(14), the dispersion pattern is depicted in Fig. 5. The dispersed-wavelength imaging positions form an LDP, and each LDP is a snapshot of the target spectra.

According to Eqs. (5), (6), (8), and (10), the point of intersection of the two "arms" of the LDP is exactly the NDIL, both of which are $(f\tan\varphi, f\tan\phi)$. Considering that each NDIL corresponds to one target location, each LDP position also corresponds to one target location.

The relation between the NDIL and LDP is depicted in Fig. 6. It also indicates that the NDIL is exactly the point of intersection of the two "arms" of the LDP.

Once the LDP is obtained, the NDIL can be obtained. We can then estimate the target location using Eqs. (8)–(11).

When only one target is present in the field, only one LDP is obtained at a time. The DIS can locate one target based on only one LDP.

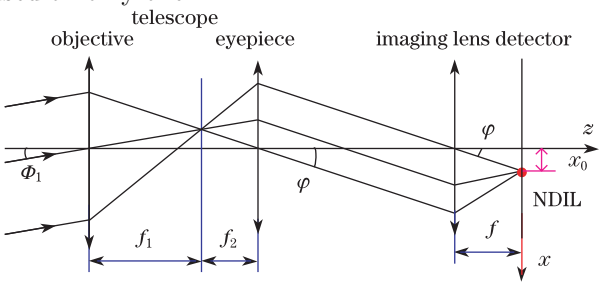

Fig. 4. Ray tracing in the sagittal plane of the DIS without the four prisms.

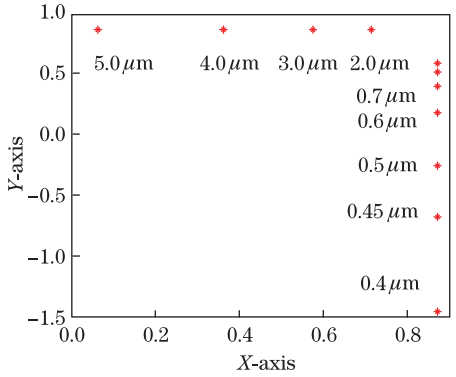

Fig. 5. (Color online) LDP ($\alpha = \beta = \pi/18$, $\gamma_1 = \pi/5.4$, $\gamma_2 = \pi/10$, $f = 50$ mm, and $\phi = \varphi = \pi/180$).

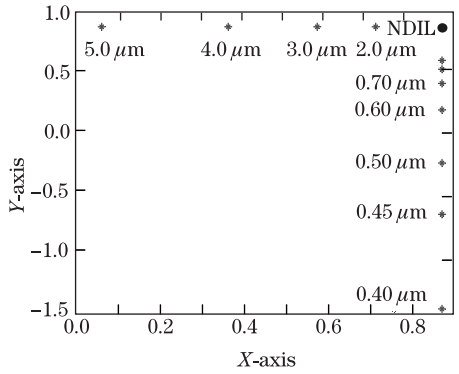

Fig. 6. (Color online) Relation between the NDIL and LDP ($\alpha = \beta = \pi/18$, $\gamma_1 = \pi/5.4$, $\gamma_2 = \pi/10$, f=50 mm, and $\phi = \varphi = \pi/180$).

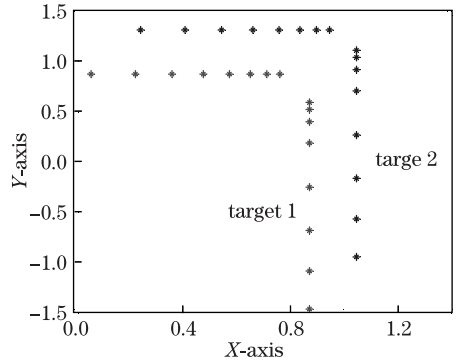

Fig. 7. (Color online) LDP of two targets ($\alpha = \beta = \pi/18$, $\gamma_1 = \pi/5.4$, $\gamma_2 = \pi/10$, and f=50 mm): target 1 ($\phi_1 = \varphi_1 = \pi/180$) and target 2 ($\phi_2 = \pi/120$, $\varphi_2 = \pi/150$).

When two targets are present in the field, two LDPs can be obtained at a time (Fig. 7). Two LDP positions correspond to two target locations. The DIS can locate two targets using only one frame of data.

The DIS may have a spectral resolution of 10 nm for the visible range and 15 nm for the mid-wave infrared range. If the material of the prism is known, two methods can be used to improve the spectral resolution. The first method increases the vertex angle of the prism, whereas the second method increases the effective length of the base of the prism.

The DIS has several advantages. Firstly, it can locate multiple targets using only one frame of data. Therefore, the DIS can locate multiple targets in real time with its rapid data acquisition and processing. Secondly, the DIS has a very broad spectral range (from 0.4 to 5.0 μm). Thirdly, the DIS has sub-pixel location accuracy for measuring targets whose energy is present in the two "arms" of the LDP. Fourthly, the DIS has no moving parts.

In conclusion, a conceptual DIS is described. A target is mapped onto the detector to form an LDP. Each LDP is a snapshot of the target spectra. The formulas and numerical simulation of the LDP are presented. The DIS is suitable for detecting and locating energetic targets in real time.

This work was supported by the Fundamental Research Funds for the Central Universities under Grant No. K5051305003.

References

1. M. V. R. K. Murty, J. Opt. Soc. Am. **50,** 7 (1960).
2. G. Guelachvili, Appl. Opt. **16,** 2097 (1977).
3. L. Genzel and J. Kuhl, Appl. Opt. **17,** 3304 (1978).
4. W. H. Steel, *Interferometry* (Cambridge University Press, Cambridge, 1983).
5. G. Durry and G. Guelachvili, Appl. Opt. **34,** 1971 (1995).
6. J. Kauppinen and V. M. Horneman, Appl. Opt. **30,** 2575 (1991).
7. J. Kauppinen, J. Heinonen, and I. Kauppinen, Appl. Spectrosc. Rev. **39,** 99 (2004).
8. P. R. Griffiths and J. A. de Haseth, *Fourier Transform Infrared Spectrometry* (Wiley-Interscience, New Jersey, 2007).
9. Q. Yang, R. Zhou, and B. Zhao, Appl. Opt. **47,** 2486 (2008).
10. Q. Yang, R. Zhou, and B. Zhao, Appl. Opt. **47,** 2186 (2008).
11. Q. Yang, R. Zhou, and B. Zhao, J. Opt. A Pure Appl. Opt. **11,** 015505 (2009).
12. Q. Yang, Appl. Opt. **49,** 4088 (2010).
13. D. F. Murphy and D. A. Flavin, Meas. Sci. Technol. **21,** 094031 (2010).
14. T. A. Al-Saeed and D. A. Khalil, Appl. Opt. **48,** 3979 (2009).
15. T. A. Al-Saeed and D. A. Khalil, Appl. Opt. **50,** 2671 (2011).
16. C. Meneses-Fabian and U. Rivera-Ortega, Opt. Lett. **36,** 2417 (2011).
17. Q. Yang, B. Zhao, and D. Wen, Opt. Laser. Technol. **44,** 1256 (2012).
18. Q. Yang, B. Zhao, and X. Zeng, Chin. Opt. Lett. **11,** 021202 (2013).
19. J. M. Mooney, Proc. SPIE **2480,** 65 (1995).
20. J. M. Mooney, V. E. Vickers, M. An, and A. K. Brodzik, J. Opt. Soc. Am. A **14,** 2951 (1997).
21. J. E. Murguia, T. D. Reeves, J. M. Mooney, W. S. Ewing, F. D. Shepherd, and A. K. Brodzik, Proc. SPIE **4028,** 457 (2000).
22. M. M. Weeks, J. E. Murguia, J. M. Mooney, R. J. Nelson, and W. S. Ewing, Proc. SPIE **5580,** 487 (2005).
23. F. D. Shepherd, J. M. Mooney, T. E. Reeves, D. S. Franco, J. E. Murguia, C. Wong, P. Dumont, F. Khaghani, G. Diaz, M. M. Weeks, and D. Leahy, Proc. SPIE **6660,** 66600J (2007).
24. F. D. Shepherd, J. M. Mooney, T. E. Reeves, P. Dumont, M. M. Weeks, and S. DiSalvo, Proc. SPIE **7055,** 705506 (2008).
25. M. Bass, G. Li, and E. V. Stryland, *Handbook of Optics* (4th edition) (McGraw-Hill, NewYork, 2009).